Chinese Chemical Letters 36 (2025) 109643

Contents lists available at ScienceDirect

Chinese Chemical Letters

journal homepage: www.elsevier.com/locate/cclet

Ultrafast synthesis of $Na_3V_2(PO_4)_3$ cathode for high performance sodium-ion batteries

Ruofan Yin[a,1], Zhaoxin Guo[b,1], Rui Liu[b], Xian-Sen Tao[a,*]

[a] School of Chemistry, Chemical Engineering and Materials, Jining University, Qufu 273155, China
[b] School of Materials Science and Engineering, Shandong University of Science and Technology, Qingdao 266590, China

ARTICLE INFO

Article history:
Received 1 January 2024
Revised 23 January 2024
Accepted 7 February 2024
Available online 12 February 2024

Keywords:
Sodium-ion batteries
Cathode materials
$Na_3V_2(PO_4)_3$
High-temperature shock
Cycling stability

ABSTRACT

$Na_3V_2(PO_4)_3$ (NVP) is regarded as alternative cathode material for sodium-ion batteries (SIBs) due to its potential high-rate performance and pronounced long-term cycle stability. However, electronic conductivity and tap density are difficult to be balanced. Herein, we report that high-temperature shock (HTS) can prepare "single crystalline like" NVP which combines high-rate capability with high tap density together into one with the assistance of carbon framework and large particle. Thus, high reversible capacity of 110 mAh/g at 0.1 C with 89.9% capacity retention after 1600 cycles at 1 C and specific capacity of 83.5 mAh/g at 50 C rate has been exhibited. This study provides a novel strategy to guide the production of high tap density, and rate performance polyanionic cathode materials.

© 2024 Published by Elsevier B.V. on behalf of Chinese Chemical Society and Institute of Materia Medica, Chinese Academy of Medical Sciences.

Lithium-ion batteries (LIBs) have been widely used in energy storage. However, the shortage of lithium supply leads to increasing price for LIBs [1,2]. Sodium-ion batteries (SIBs), owing to the abundant resources and widespread geological distribution of sodium, are regarded as LIBs substitutes especially in low-speed electric vehicles and large-scale energy storage systems [3–5]. $Na_3V_2(PO_4)_3$ (NVP), with a fast Na^+-transportable NASICON framework, has attracted ubiquitous attention as the alternative cathode material due to potential rate performance and pronounced long-term cycle stability [6]. While, the inherent low electronic conductivity limits the electrochemical performances particularly in high-rate capability [7,8].

To enhance the rate capability, carbon-coating technique has been applied to improve the electric conductivity. However, carbon limits the particle growth of NVP, which usually results in the small size of NVP and low tap density [9–11]. Single crystal design can improve the tap density, reduce the specific surface area of cathode, and reduce the side reactions between cathode and electrolyte [12], and thus widely explored in SIBs [13]. Unfortunately, the inhibitory effect of the carbon layer on single crystal growth makes the direct preparation of large-sized single crystals in combination with carbon a significant challenge [14]. Based on the above points, it is necessary to develop a simple but effective method that ensures both the formation of a well-established carbon framework and the growth of single crystals, aiming to obtain sodium-ion cathode materials with both high tap density and high electrochemical performance for industrial applications.

Herein, we propose a single crystalline-like strategy preparing NVP with carbon framework achieved by high-temperature shock (HTS) within ~15 s (Scheme 1). Namely, through a simple solid-state one-pot reaction, the single-crystalline-like NVP materials with a carbon framework and with a size larger than 50 μm were synthesized, which was similar to the size of reported single crystalline NVP prepared by the tube furnace (TF) [14]. It has come to our attention that in previous studies, polymer stabilized droplet templating method was employed for the preparation of single crystalline NVP [14,15], which is characterized by its time-consuming nature and complicated procedures. As a comparison, HTS could efficient prepare single crystalline like NVP materials in an extremely short time. Moreover, HTS has remained the morphology of NVP precursor and the structure of carbon. Furthermore, a novel carbon framework has been created which results in low charge-transfer resistance and excellent dynamic performance. Specifically, the single-carystal-like NVP with carbon framework could deliver 83.5 mAh/g at 50 C. Moreover, it has impressive long-term cycle stability (89.9% after 1600 cycles at 1 C) in half-cell. In addition, the single-carystal-like NVP with carbon framework exhibits high electrochemical performance in full-cell test. This work presents an innovative strategy for the ultrafast preparation of high tap density, high-performance, single-crystalline-like NVP, as well as high-energy-density polyanion cathode materials for SIBs.

* Corresponding author.
E-mail address: taoxsen@jnxy.edu.cn (X.-S. Tao).
[1] These authors contributed equally to this work.

https://doi.org/10.1016/j.cclet.2024.109643
1001-8417/© 2024 Published by Elsevier B.V. on behalf of Chinese Chemical Society and Institute of Materia Medica, Chinese Academy of Medical Sciences.

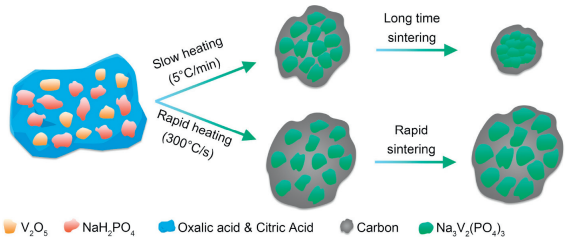

Scheme 1. Schematic illustration for the synthesis of NVP with HTS or TF.

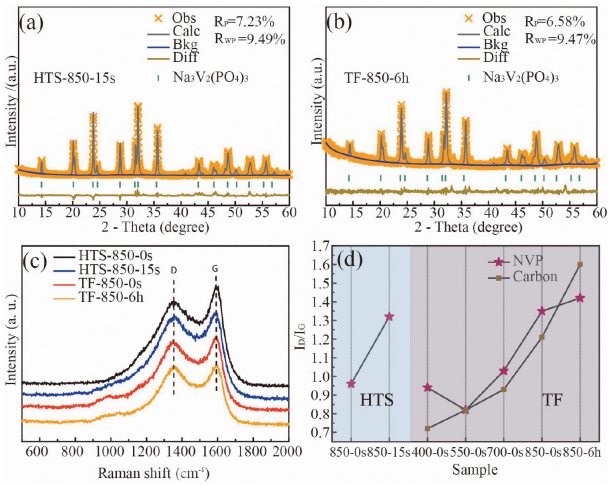

Fig. 1. The XRD Rietveld refinements of (a) HTS-850–15s and (b) TF-850–6h. (c) Raman spectrum of HTS-850–0s, HTS-850–15s, TF-850–0s, and TF-850–6h. (d) I_D/I_G of samples synthesized at different conditions.

The synthesis process of NVP with carbon framework is shown in Scheme 1. Briefly, V_2O_5, NaH_2PO_4, oxalic acid and citric acid were mixed through ball-milling method (experimental details are exhibited in Supporting information). And then the mixture was placed on the HTS equipment (Fig. S1 in Supporting information) for a high-temperature shock with heat retention and for 0 s and 15 s in an argon atmosphere at 850 °C to obtain sample HTS-850–0s and HTS-850–15s, respectively. For comparison, the mixtures were also placed in a tube furnace and calcined at 800 °C under argon atmosphere for 0 s, 6 h to prepare TF-850–0s and TF-850–6h. Fig. 1 depicts the XRD patterns and Raman spectroscopy of as-prepared NVP products, respectively. As shown in Figs. 1a and b and Fig. S2 (Supporting information), all XRD patterns are indexed to highly crystalline rhombohedra phase ($R\bar{3}$ *c* space group), and no impurities are detected, indicating the successful preparation of NVP materials. Tables S1-S4 (Supporting information) show the refined cell parameters of the prepared four NVP samples. And it is evident that there is a minimal difference in lattice parameters between materials prepared by HTS and those prepared by the tube furnace calcination, agreeing with previous reports [16,17]. Meanwhile, Raman spectra was performed to investigate the surface features of four products (Fig. 1c). Two types of carbon bands centered at 1346 and 1593 cm^{-1} are attributed to the D (disorder carbon, sp^3-coordinated behavior) and G (crystalline graphitized carbon, sp^2-coordinated behavior) bands of carbon, respectively. The peak intensity ratios of D to G band of HTS-850–0s, HTS-850–15s, TF-850–0s and TF-850–6h was calculated, with a value of 0.96, 1.32, 1.35, and 1.42, respectively. Obviously, HTS-850–0s presents lowest value of I_D/I_G, indicating the carbon with sp^2-coordinated behavior is predominant. This may be due to the short reaction time and the temperature for HTS-850–0s is unfavorable for carbonization, leading to the abundant presence of

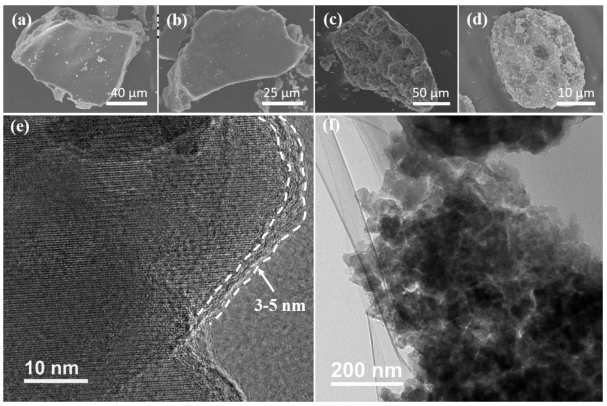

Fig. 2. SEM images of (a) HTS-850–0s, (b) HTS-850–15s, (c) TF-850–0s, (d) TF-850–6h. (e, f) TEM images of HTS-850–15s.

the sp^2 carbon, such as carbon-carbon double bonds, possibly due to the catalytic reaction of carbon precursors by vanadium element in NVP under inert atmosphere and high-temperature conditions [18,19]. To demonstrate this reaction process, NVP synthesized with TF at different temperatures and TF samples for carbon sources were supplemented, and their Raman spectra were analyzed (Fig. 1d). As the temperature and holding time increase, the value of I_D/I_G shows an upward trend, which may be attributed to the transformation of sp^2 carbon to sp^3 carbon with the increasing degree of aromatization and polycondensation [18]. In addition, determined from infrared carbon & sulfur analyzers, the carbon contents of HTS-850–0s, HTS-850–15s, TF-850–0s and TF-850–6h are 4.99, 6.14, 7.52, 6.26 wt%, respectively.

The morphology and size of HTS-850–0s, HTS-850–15s, TF-850–0s, and TF-850–6h were characterized by scanning electron microscope (SEM), respectively. As shown in Figs. 2a-d, HTS-850–0s, HTS-850–15s, and TF-850–0s exhibit the similar size with NVP precursor (Fig. S3 in Supporting information), all larger than 50 μm, while TF-850–6h shows smaller size. Additionally, HTS-850–0s and HTS-850–15s show smooth and flat particle surface as well as NVP precursor, which like the morphology of single crystal [20–22], while TF-850–0s and TF-850–6h exhibit rough surface. This may be due to the ultrafast heating rate and short sintering time which result in the incomplete decomposition of carbon coating in HTS-850–0s and HTS-850–15s [18]. Whereas, complete decomposition of carbon coating, and neck growth at low temperatures without densification in sintering leads to the morphology which shown as TF-850–0s and TF-850–6h (Figs. 2c and d) [23]. The high-resolution transmission electron microscope (HRTEM) image (Fig. 2e and Fig. S4a) reveals a *ca.* 3–5 nm carbon layer on HTS-850–15s and 8–10 nm carbon layer on TF-850–6h, which could protect NVP from electrolyte erosion and enhance dynamic performance. Moreover, carbon tends to form carbon framework in HTS-850–15s (Fig. 2f) while agglomerating on the surface of NVP particle in TF-850–6h (Fig. S4b). Additionally, as shown in Figs. 2e and f, secondary particles are aggregated by primary particles linked through carbon framework in HTS-850–15s. This is distinct from TF-850–6h materials, which are solely coated with carbon. The variation in thickness and morphology of carbon species may be attributed to the different heating and holding conditions during the production of HTS-850–15s and TF-850–6h samples.

Fig. 3 exhibits the electrochemical performances of half-cells for all samples. Fig. 3a exhibits the galvanostatic charge-discharge curves at 0.1 C (1 C = 117 mA/g). All electrodes display a voltage plateau around 3.4 V which corresponds to the redox of V^{3+}/V^{4+}. Meanwhile, the four materials exhibit similar initial reversible capacity. Specifically, 110.6 mAh/g (HTS-850–0s), 110.0 mAh/g (HTS-

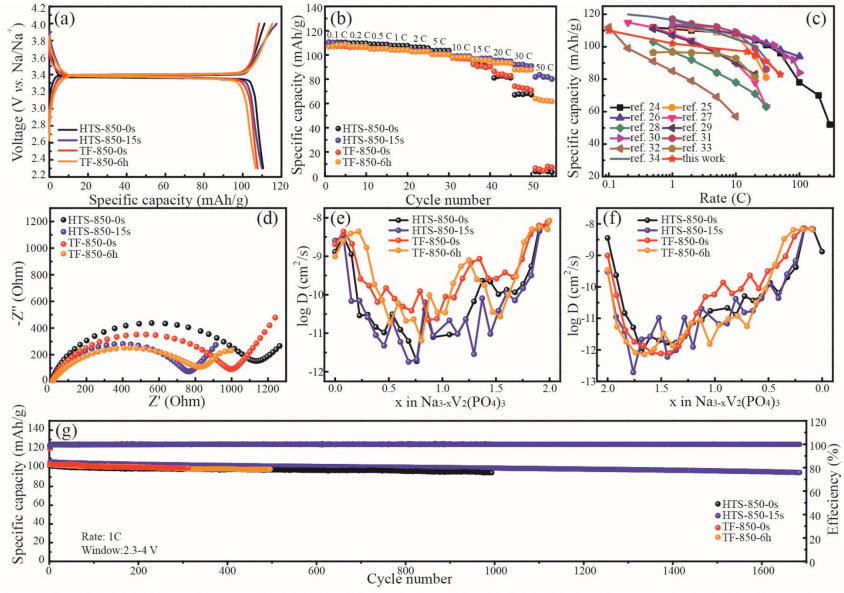

Fig. 3. Electrochemical performance of HTS-850–0s, HTS-850–15s, TF-850–0s, and TF-850–6h. (a) Charge-discharge profiles at a current rate of 0.1 C. (b) Rate performances from 0.1 C to 50 C at voltage window of 2.3–4 V. (c) Comparison of rate performance of HTS-850–15s to the recent results in the literature for NVP. (d) Electrochemical impedance spectra. (e) Comparation of Na^+ diffusion coefficient calculated by GITT at charge process. (f) Comparation of Na^+ diffusion coefficient calculated by GITT at discharge process. (g) Cycling performance at 1 C.

850–15s), 107.7 mAh/g (TF-850–0s) and 106.7 mAh/g (TF-850–6h). Fig. 3b displays the rate performances of HTS-850–0s, HTS-850–15s, TF-850–0s and TF-850–6h. All NVP materials deliver comparable discharge capacity at the rate of 0.1, 0.2, 0.5, 1, 2, 5 and 10 C. However, HTS-850–15s (97.1 mAh/g) and TF-850–6h (96.2 mAh/g) display higher reversible capacity compared to the other samples at 15 C. Meanwhile, the more obvious differences started at 30 C (Fig. 3b, Figs. S5 and S6 in Supporting information). HTS-850–15s (91.3 mAh/g) exhibits the highest reversible capacity, followed by TF-850–6h (87.8 mAh/g), TF-850–0s (74.2 mAh/g) and HTS-850–0s (68.4 mAh/g). Even at a high rate of 50 C, HTS-850–15s still exhibits a high specific capacity of 83.5 mAh/g. Comparison of rate performance of HTS-850–15s to the recent results in the literature for NVP is displayed in Fig. 3c and Table S5 (Supporting information) [24–34]. Obviously, the HTS-850–15s material's performance is at the mainstream level among all the listed samples. Additionally, EIS is carried out to investigate internal impedance. The semicircles at medium frequency are associated with charge-transfer resistance at the interface (R_{ct}). As shown in Fig. 3d, HTS-850–15s exhibits the lowest R_{ct}, caused by the unique carbon framework, resulting in the best rate performance. Moreover, GITT was employed to estimate the Na^+ diffusion coefficient in four samples (Fig. S7 in Supporting information). As shown in Figs. 3e and f, the Na^+ diffusion coefficient of HTS-850–0s and HTS-850–15s seems lower in charge-discharge process, which might result from the long Na^+ diffuse path in large particle size [20–22]. And the rate results (Fig. 3b) and previous study in other literature [35] has proved that the lower Na^+ diffusion coefficient is not in contradiction with the high rate performance of NVP. In Fig. 3g, superior capacity retention had been demonstrated among all samples at 1 C. HTS-850–15s delivers a high capacity retention with 89.9% after 1600 cycles and nearly 100% Coulombic efficiency was achieved among the whole cycle life. Besides, higher tap density ($\approx$0.98 g/cm^3) for HTS-NVP has been measured in Table S6 (Supporting information), which matches the results of NVP particle size and cycle stability.

To further demonstrate the practical application of the prepared NVP materials, full-cells were assembled with HTS-850–15s cathode and presodiated hard carbon (HC) anode, abbreviated as

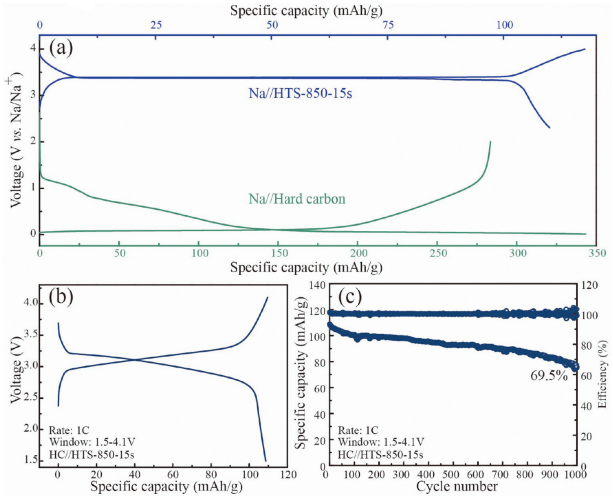

Fig. 4. Electrochemical behavior of HC//HTS-850–15s full-cells. (a) The charge-discharge profiles of HTS-850–15s cathode and commercial hard carbon anode in half cell. (b) The charge-discharge profiles of HC//HTS-850–15s. (c) Cycling performance at 1 C.

HC//HTS-850–15s. As shown in Fig. 4a, the charge/discharge curves of HTS-850–15s exhibit a voltage plateau around 3.4 V and the reversible specific capacity of 110 mAh/g in half-cell test, while the hard carbon exhibits continuous charge/discharge curves with the reversible specific capacity of 283.5 mAh/g. And the HC//HTS-850–15s full-cell exhibits initial discharge specific capacity of 108.7 mAh/g at 1 C (Fig. 4b). After 1000 cycles, the full-cell still exhibits 75.6 mAh/g with high capacity retention (69.5%), exhibiting good cycling stability (Fig. 4c). As shown in Fig. S8 (Supporting information), the capacity fade was not caused by HTS-850–15s cathode. The results indicate the as-prepared NVP materials are feasible for practical SIBs application.

In this work, a single crystalline like NVP with excellent long cycle stability, outstanding rate performance, and high tap density has been developed using HTS and solid-state one-pot reac-

tion method for SIBs application. Combining SEM and TEM, we conclude that the impressive performance own to the unique carbon framework and large particle size. HTS-850–15s delivers a high reversible capacity of 110 mAh/g and 89.9% capacity retention after 1600 cycles and nearly 100% Coulombic efficiency among the whole cycle life. This work raises a new strategy for the production of high tap density, and outstanding electrochemical performance polyanionic cathode materials for SIBs.

Declaration of competing interest

The authors declare that they have no known competing financial interests or personal relationships that could have appeared to influence the work reported in this paper.

Acknowledgments

This work was supported by the National Natural Science Foundation of China (No. 22109091) and Natural Science Foundation of Shandong Province (No. ZR2021QB180).

Supplementary materials

Supplementary material associated with this article can be found, in the online version, at doi:10.1016/j.cclet.2024.109643.

References

[1] P.K. Nayak, L. Yang, W. Brehm, P. Adelhelm, Angew. Chem. Int. Ed. 57 (2018) 102–120.
[2] Z. Guo, G. Qian, C. Wang, et al., Prog. Nat. Sci. 33 (2023) 1–7.
[3] L. Shen, Y. Li, S. Roy, et al., Chin. Chem. Lett. 32 (2021) 3570–3574.
[4] J. Feng, S. Luo, K. Cai, X. Liu, et al., Chin. Chem. Lett. 33 (2022) 2316–2326.
[5] K. Liang, D. Wu, Y. Ren, X. Huang, J. Ma, Chin. Chem. Lett. 34 (2023) 107978.
[6] Z. Jian, Y.S. Hu, X. Ji, W. Chen, Adv. Mater. 29 (2017) 1601925.
[7] Q. Wang, S. Chu, S. Guo, Chin. Chem. Lett. 31 (2020) 2167–2176.
[8] N.T. Aristote, K. Zou, A. Di, et al., Chin. Chem. Lett. 33 (2022) 730–742.
[9] Y. Xu, Q. Wei, C. Xu, et al., Adv. Energy Mater. 6 (2016) 1600389.
[10] Y.L. Zhao, X.X. Cao, G.Z. Fang, et al., Chem. Eng. J. 339 (2018) 162–169.
[11] X.H. Liu, E.H. Wang, G.L. Feng, et al., Electrochim. Acta 286 (2018) 231–241.
[12] L. Ni, S. Zhang, A. Di, et al., Adv. Energy Mater. 12 (2022) 2201510.
[13] J. Lamb, K. Jarvis, A. Manthiram, Small 18 (2022) 2106927.
[14] H. Xiong, G. Sun, Z. Liu, et al., Angew. Chem. Int. Ed. 60 (2021) 10334–10341.
[15] M. Su, J. Shi, Q. Kang, et al., Chem. Eng. J. 432 (2022) 134289.
[16] Z. Tian, Y. Chen, J. Cheng, et al., Ceram. Int. 47 (2021) 22025–22034.
[17] R.S. Kate, S.V. Kadam, M.V. Kulkarni, et al., J. Energy Storage 74 (2023) 109245.
[18] X.W. Dou, I. Hasa, D. Saurel, et al., Mater. Today 23 (2019) 87–104.
[19] R.R. Langeslay, D.M. Kaphan, C.L. Marshall, et al., Chem. Rev. 119 (2019) 2128–2191.
[20] F. Zhang, S. Lou, S. Li, et al., Nat. Commun. 11 (2020) 3050.
[21] X. Fan, X. Ou, W. Zhao, et al., Nat. Commun. 12 (2021) 5320.
[22] X. Ou, T. Liu, W. Zhong, et al., Nat. Commun. 13 (2022) 2319.
[23] C. Wang, W. Ping, Q. Bai, et al., Science 368 (2020) 521–526.
[24] Y. Fang, L. Xiao, X. Ai, Y. Cao, H. Yang, Adv. Mater. 27 (2015) 5895–5900.
[25] Y. Jiang, Z. Yang, W. Li, et al., Adv. Energy Mater. 5 (2015) 1402104.
[26] W. Ren, Z. Zheng, C. Xu, et al., Nano Energy 25 (2016) 145–153.
[27] J. Zhang, Y. Fang, L. Xiao, et al., ACS Appl. Mater. Interfaces 9 (2017) 7177–7184.
[28] Q. Ni, Y. Bai, Y. Li, et al., Small 14 (2018) 1702864.
[29] J. Zhang, W. Liu, H. Hu, et al., Electrochim. Acta 292 (2018) 736–741.
[30] Y. Jiang, X. Zhou, D. Li, et al., Adv. Energy Mater. 8 (2018) 1800068.
[31] P.N. Didwal, R. Verma, C.W. Min, C.J. Park, J. Power Sources. 413 (2019) 1–10.
[32] S.K. Pal, R. Thirupathi, S. Chakrabarty, S. Omar, ACS Appl. Energy Mater. 3 (2020) 12054–12065.
[33] M. Jiang, D. Xu, B. Yang, C. Zhang, M. Cao, Adv. Mater. Interfaces 8 (2021) 2100188.
[34] L. Liang, X. Li, F. Zhao, et al., Adv. Energy Mater. 11 (2021) 2100287.
[35] X. Jiang, T. Zhang, J.Y. Lee, J. Power Sources 372 (2017) 91–98.